J Nanostruct 16(1): 839-848, Winter 2026

RESEARCH PAPER

# Electrochemical Polymerization for Tyramide Derivative for Solar Cell Application

*Noor Ali Khudhair [1], Sana Adnan Habeeb [2], Mayasa Issam Ali [1] **

[1] *Department of chemistry, College of science, University of Baghdad, Baghdad, Iraq*

[2] *Department of chemistry, College of Education for pure science (IbnAl-Haitham), University of Baghdad, Baghdad, Iraq*

## ARTICLE INFO

***Article History:***
*Received 18 September 2025*
*Accepted 19 December 2025*
*Published 01 January 2026*

***Keywords:***
*Dye Sensitized Solar Cell*
*Electrochemical Polymerization*
*Eosin Dye*
*Graphene*
*Poly Tyramide Derivative*

## ABSTRACT

This paper includes synthesis of coating polymer derivative of amide by Electropolymerization technique that include Tyramide derivative. Tyramide derivative is prepared in the presented work for serving as poly tyramide in dye sensitized solar cell (DSSC). Through the use of the Scanning Electron Microscope (SEM), Fourier Transform Infraranded (FT-IR), Atomic Force Microscope (AFM) and X-Ray Diffraction (XRD) inspections revealed data on particle size, shape and the structure. The results indicate to the interaction between the polymer and nanomaterial (Graphene). Using the electrochemical polymerization process, poly Tyramide derivative film (counter electrode) is prepared. Poly Tyramide derivative film is modified with Graphene to increase the efficiency of film in dye sensitized solar cell. The dye is used in this study is eosin dye. For poly Tyramide derivative film modified with Graphene, the efficiencies are 3.1% and 5.9%, respectively. In the fabrication of DSSCs, this provided economy preference to poly Tyramide derivative film on Graphene.

**How to cite this article**
*Khudhair N., Habeeb S., Ali M. Electrochemical Polymerization for Tyramide Derivative for Solar Cell Application. J Nanostruct, 2026; 16(1):839-848. DOI: 10.22052/JNS.2026.01.074*

## INTRODUCTION

A solar cell can be defined as a photovoltaic (PV) device which converts the energy of light to electrical energy. In particular, ETM (i.e., electron transport material) of a DSSC is made of a wide band gap semi-conductor that is deposited over a transparent conductive oxide (TCO) glass. The dye molecule is after that anchored to semiconductor surface as charge layer that can absorb visible light in dye region as well as transfer photo charges to hole- and electron- conducting materials. A redox-coupled electrolyte, usually consisting of iodide/ triiodide ions ($I^-/I_3^-$), is known as the hole transport material (HTM). It contacts to a cathode or counter electrode (CE), in which oxidized donor reduction occurs. These days, the final PV efficiency of solar cells greatly depends on development of CEs for DSSCs. It is vital to identify alternative inexpensive and noble metal - free materials for replacing Pt in the DSSCs, and conducting polymers appear to have intriguing potential [2,3]. The first step is crucial in producing ionic conductivity (I-), which speeds up redox process and aids in the oxidized dye's quicker rate of regeneration. Second, it is

* *Corresponding Author Email: maiassa.ali@sc.uobaghdad.edu.iq*

caging more cations, which raises the potential and causes the dye's positive molecular orbital (HOMO) to shift downward [4]. This contributes to electron recombination rate reduction between holes in the dye's HOMO and electrons in $TiO_2$ conduction band. Moreover, pyridine is used as a donating material, which modifies $TiO_2$ surface charge, shifting its conduction band upward and raising the open circuit voltage (Voc). The PV efficiency, which is defined as [5], is increased by this configuration by raising open circuit voltage (Voc). Fig. 1 illustrated DSSC principle [6–10]. Typically, excited state electrons inject semiconductor's conduction band (CB) and then move across external circuit to counter electrode. In order to create reduced electrolyte and achieve electrolyte regeneration, oxidized electrolyte takes electrons from counter electrode; At interfaces of such three parts, electron recombination ions take place. In this regard, the three DSSC parts play essential and indispensable roles in determining how well the device performs. The selection and production of component materials are essential. The polymers could be utilized for fabricating flexible substrates, to create a mesoporous electrode structure, for preparing a polymer gel electrode, and catalyzing electrolyte reduction as counter electrodes.

## MATERIALS AND METHODS

*Preparation of electrolyte*

Gel- electrolyte was prepared by using Polyethylene glycol (PEG 4000) as high-molecular additive, KI as iodide, ACN as solvent, and I2 by molecular rate of 3.0g: 15.0ml: 2 gm: 0.2 gm [11].

*Preparation of photo electrode ($TiO_2$/Dye)*

Through using the doctor blend method, $TiO_2$ has been deposited on ITO glass with a resistance of 10Ω/cm2 and sintered for 30 mins at 450°C. Fig. 2 illustrates how the working electrode ($TiO_2$ electrode) was immersed in eosin dye for 30 mins.

*Preparation of poly counter electrode*

Fig. 3 illustrates the electrochemical polymerization of Tyramide derivative (DE) onto the surface of Indium Tin oxide (ITO) in monomer solution by utilizing a DC power supply and two electrodes, the Country electrode (CE) and Working electrode (WE). Three drops of 95% $H_2SO_4$ were added to 100 milliliters of water together with 0.1 gram of Tyramide derivative as the solution used for electrochemical polymerization [12]. To improve the effectiveness of the polymer film, 0.004g of graphene was also added.

*Structural and Morphological Measurements*

The Measurements include studying the structure and the surface morphological for the prepared films and the used materials by using FTIR, AFM, and SEM.

*Fourier Transform Infrared Region Spectroscopy (FTIR)*

FTIR is an instrument to determine organic functional group for liquid, powder, gases, and

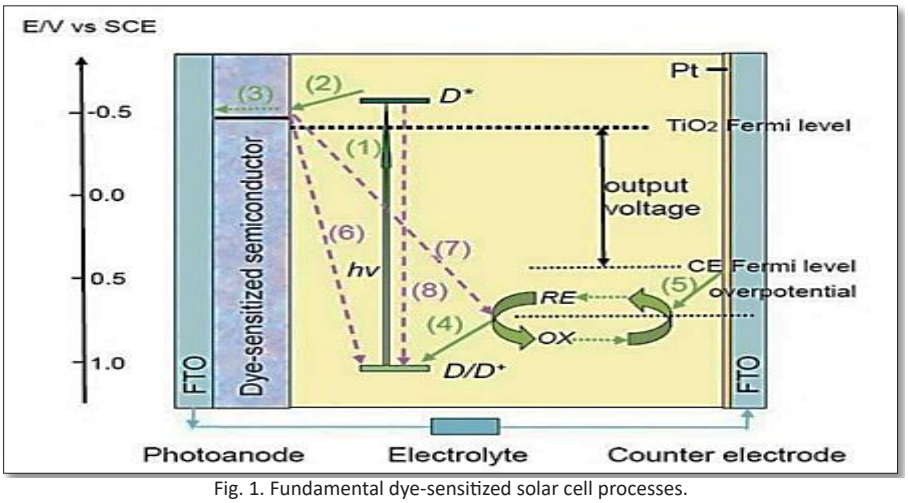


Fig. 1. Fundamental dye-sensitized solar cell processes.

Fig. 2. $TiO_2$ electrode (working electrode) immersed in eosin dye.

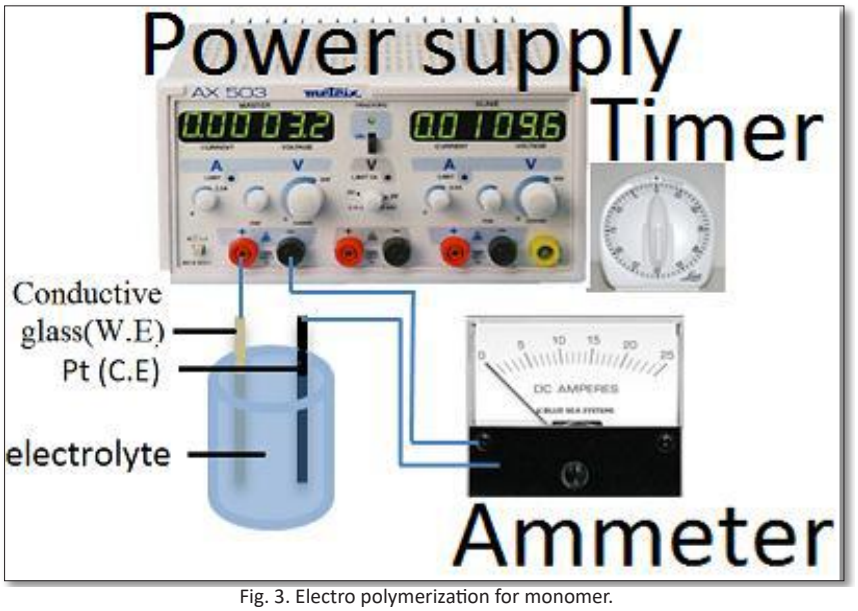


Fig. 3. Electro polymerization for monomer.

films by their structural groups. In this work this technique employed to characterize the synthesis polymer [13].

*Atomic Force Microscope (AFM)*

The cantilever utilized for scanning the specimen surface for insulating surface structure at atomic resolution has a pointed tip, or probe, at the end. The attractive force between surface and the tip is sensed during scanning, which is a dynamic process because the tip is in mechanical contact with the specimen. The surface as well as tip's Vander-Waals interaction generated such attractive force [14].

*Scanning Electron Microscope (SEM)*

The surface topography can be measured with electron beams with the use of SEM, an analytical instrument. The surface topography cannot be measured because the electron beam is concentrated from micro to nanometers through the magnetic field. Images of secondary electron (SE) or backscattered electron (BSE) modes are produced by SEM. Typically, SEM mode provided images based on topographical data [15].

*X-Ray Diffraction (XRD)*

XRD is the best method to determine the crystal structure and lattice parameters. The principle of XRD found in textbooks, such as the one by Buerger [16], Alexander and Klug [17], Cullity [139]. The studies of XRD considered the significant source to provide wide comprehension of the structure

Table 1. Spectral FTIR data for monomer.

| Functional group | Absorption bands ($cm^{-1}$) |
|---|---|
| V(O-H) phenolic | 3398.34 |
| V(O-H) carboxylic | Overlap with CH aromatic |
| V(N-H) amide | 3301.91 |
| V(C=O) carboxylic | 1706.88 |
| V(C=O) amide | 1635.52 |
| V (C-H) aromatic | 3128.32, 3056 |
| V(C-H) aliphatic | 2954.74, 2858.31 |
| V(C=C) aromatic | 1548, 1442 |

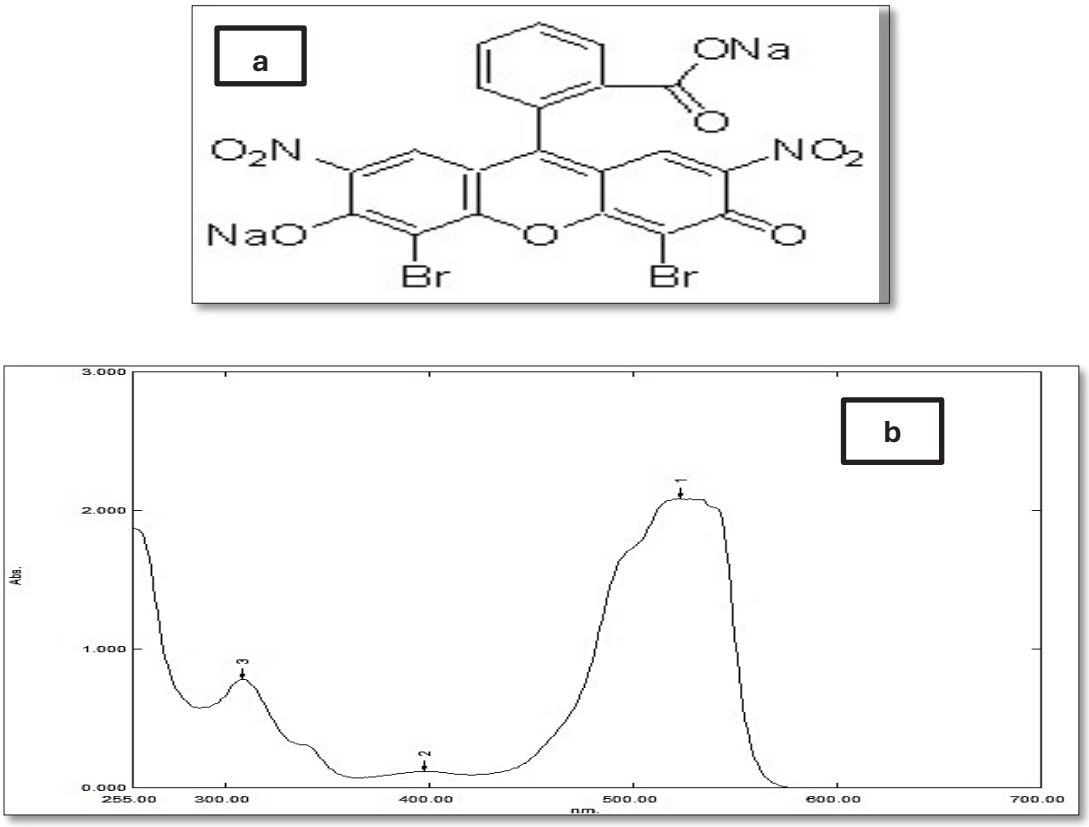


Fig. 4. (a) Chemical structure of eosin dye, (b)absorption spectrum of eosin dye.

of a molecule and the crystal structure. The Bragg spectrometer principle for such study [18]

## RESULTS AND DISCUSSION

*UV-Vis spectroscopy for Eosin dye*

The dye is used in this study is eosin dye, its chemical structure is shown in Fig. 4. The absorption spectrum of Eosin dye is exhibited in Figure. It is clear that it has absorption peaks at 523 nm,398 nm and 309 nm, which indicates that it has high transmission in these regions.

*Mechanism of polymerization*

*Characterization of poly Tyramide derivative film*

*Fourier transmittance Infrared Region (FTIR)*

Fig. 5 compares the FT-IR spectrum regarding the Tyramide derivative monomer as well as poly Tyramide derivative. FT-IR spectrophotometer (8400 max resolution 0.50cm$^{-1}$) was used in order to perform the FTIR experiments for the prepared poly Tyramide derivative. The polymer film was proven to have formed when the aliphatic double bond (CH=CH) in the monomer's spectra

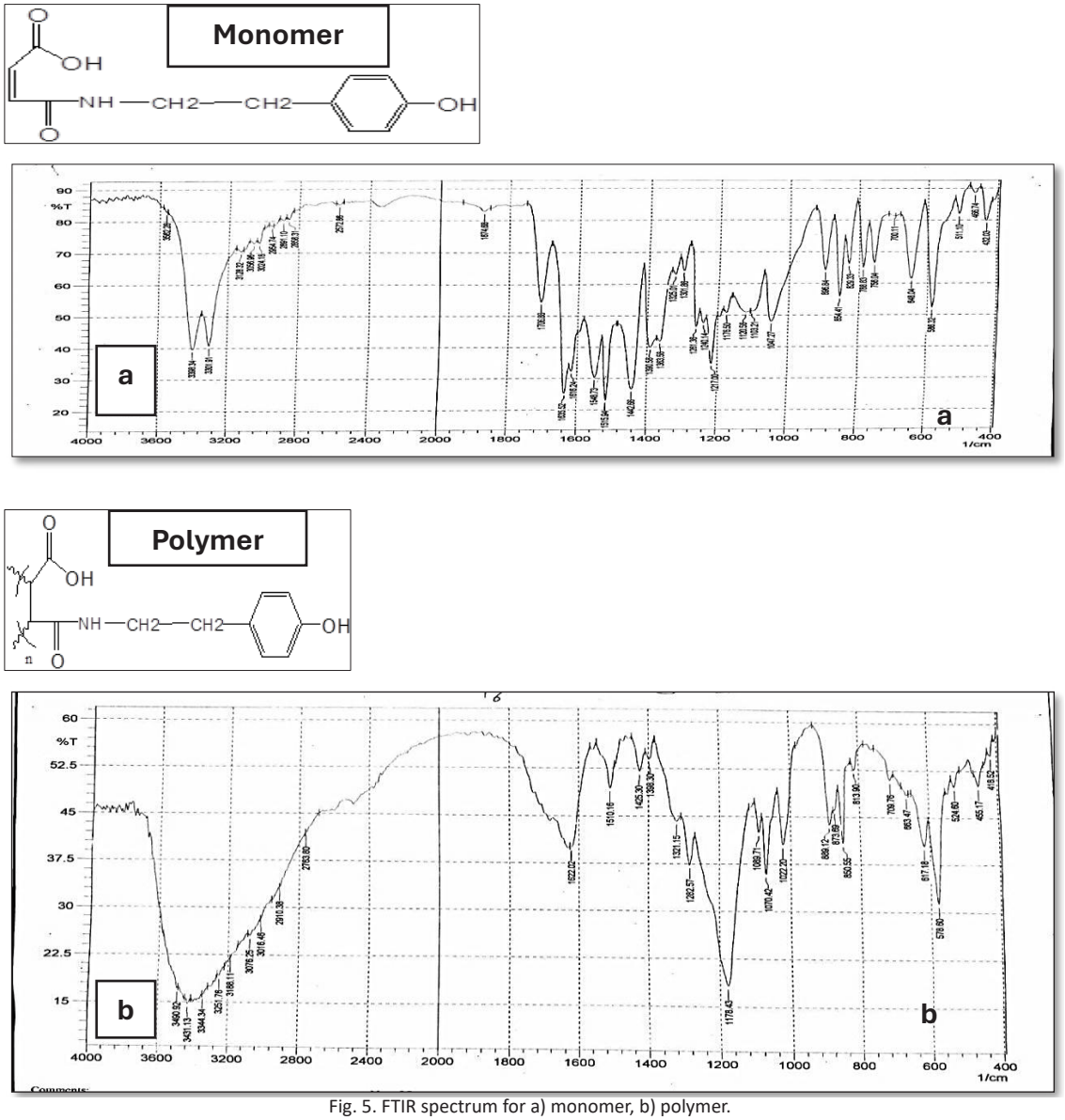


Fig. 5. FTIR spectrum for a) monomer, b) polymer.

at 1616.24 $cm^{-1}$ disappeared. Tyramide derivative monomer absorption band rates are shown in Table 1 [19].

*Scanning Electron Microscope (SEM)*

SEM was used to analyze surface morphological features of polymer film in both the presence and absence of graphene. SEM image for the polymer film, which revealed irregular distribution on the surface of S.S. with minimal porosity and compact structure, is displayed in Figs. 6a and 6b. Graphene modified polymer film, on the other hand, clearly showed particle size aggregation with a cluster poly structure on one side and a fiber-like poly structure on the other [20].

*Atomic Force microscope (AFM)*

Since AFM is regarded as one of the notable surface examination tools for nanoscale structures, it was used to gather more information due to

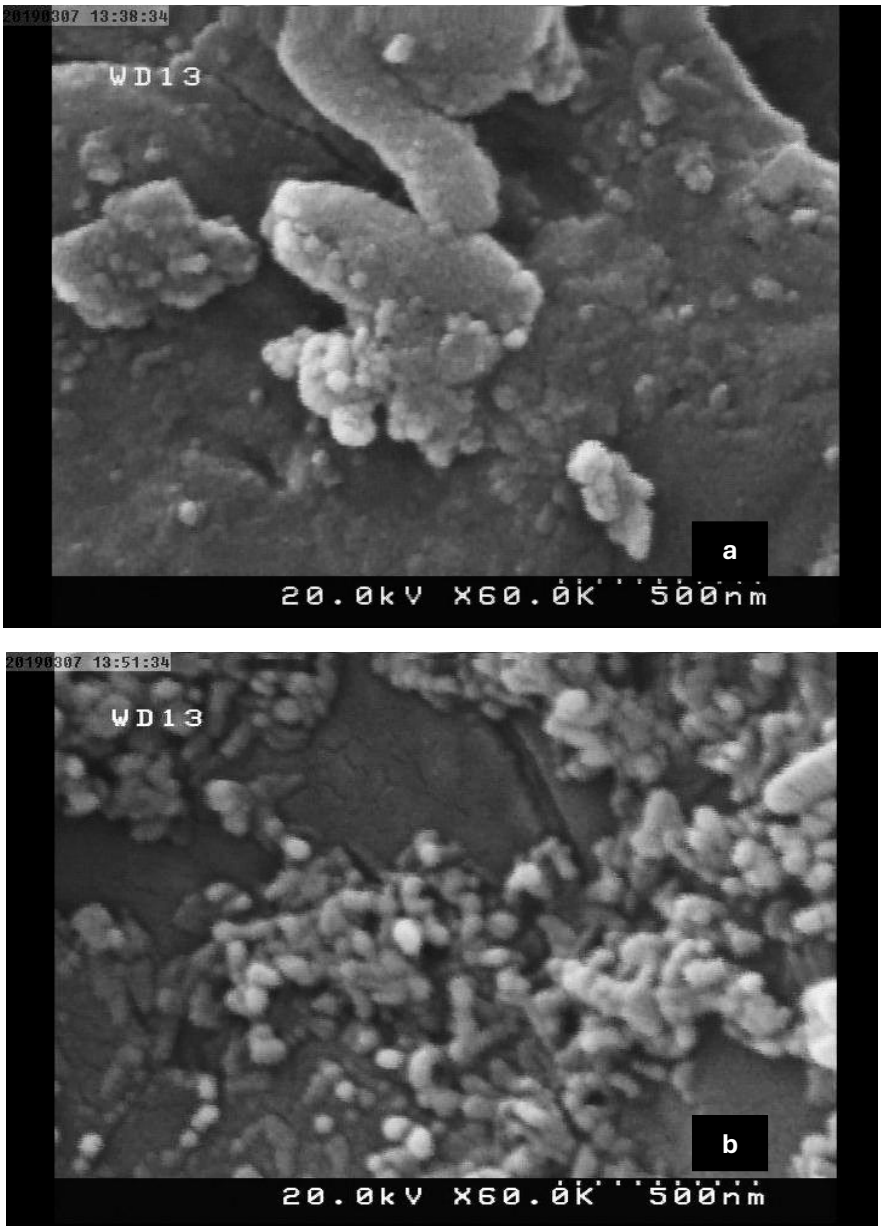


Fig. 6. SEM for a) polymer film, b) polymer film modified with Graphene

the significance of the nanomaterial's surface qualities as well as their direct impact on efficiency through application. The 3D and 2D images in Figs. 7a, and 7b illustrate the extent of nanomaterial agglomeration caused by G's adhesiveness to the polymer. The most often used metrics in AFM analysis for characterizing surface roughness for polymer films are average roughness (Ra) and root mean square roughness (RMS) [21, 22]. Table 2 provides a summary of the acquired Ra and RMS values.

*X-ray diffraction (XRD)*

XRD for Graphene, poly Tyramide derivative and poly Tyramide derivative modified with Graphene are showed in Fig. 8. XRD for Graphene is showed in Fig. 8a involve broad peaks at (2Θ = 25.07, 44.47 degree) [23]. Fig. 8b is showed XRD for poly Tyramide derivative film which involve sharp reflection peaks at (2Θ=9.58,26.6 and 28.56 degree) and that reflect its crystallite nature. Fig. 8c is showed the effect of addition of Graphene in the polymer matrix. it is showed a broad peak at (2Θ=26 degree). This peak reflected to interaction of Graphene sheets with polymer matrix.

*Characterization of assembled DSSCs*

DSSCs from mixed combination of different

Table 2. Mean grain size, Ra and RMS for polymer film in presence and absence of Graphene.

| Coating | Mean grain size (nm) | Ra(nm) | RMS (nm) |
|---|---|---|---|
| Polymer | 75.20 | 6.64 | 8.00 |
| polymer modified with Graphene | 93.98 | 2.79 | 3.48 |

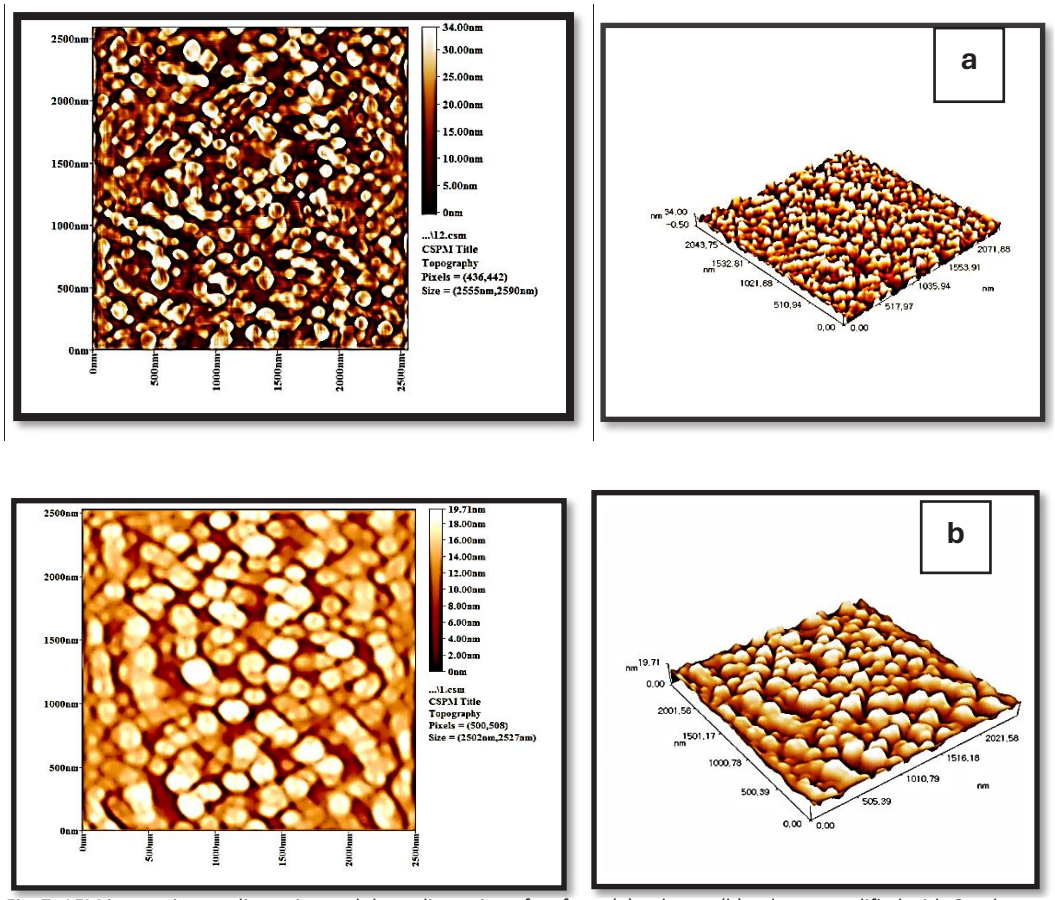


Fig. 7. AFM images in two dimension and three dimension of surfaces (a) polymer, (b) polymer modified with Graphene.

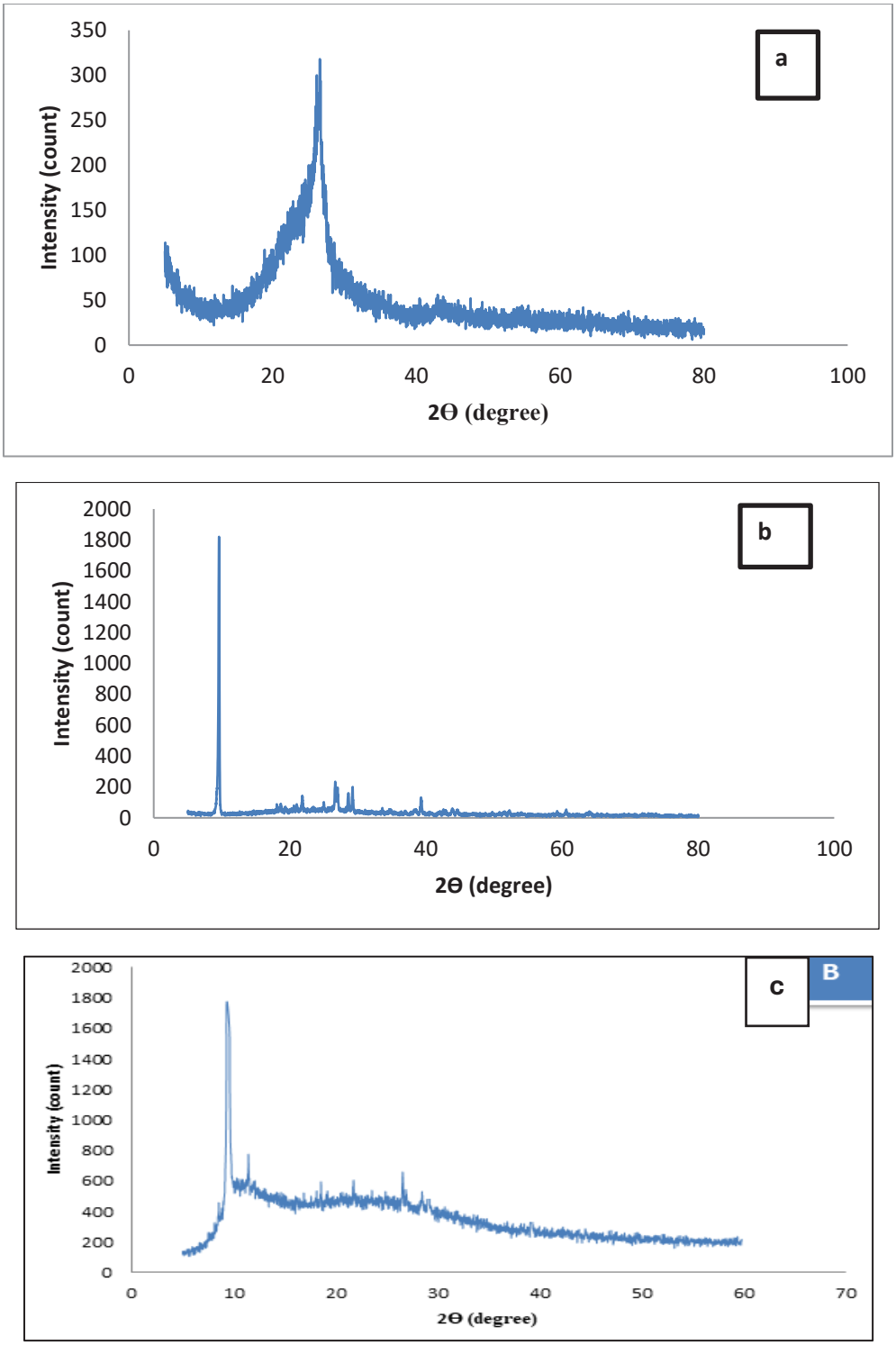


Fig. 8. XRD for (a) Graphene, (b) polymer film, (c) polymer modified with Graphene.

Table 3. Parameters of assembled DSSCs.

| Cell | Voc | Isc | Vmax | Imax | FF | E% |
|---|---|---|---|---|---|---|
| Polymer | 497 | 2.9 | 239 | 1.3 | 0.2 | 3.1 |
| Polymer modified with Graphene | 528 | 3.5 | 346 | 1.7 | 0.3 | 5.9 |

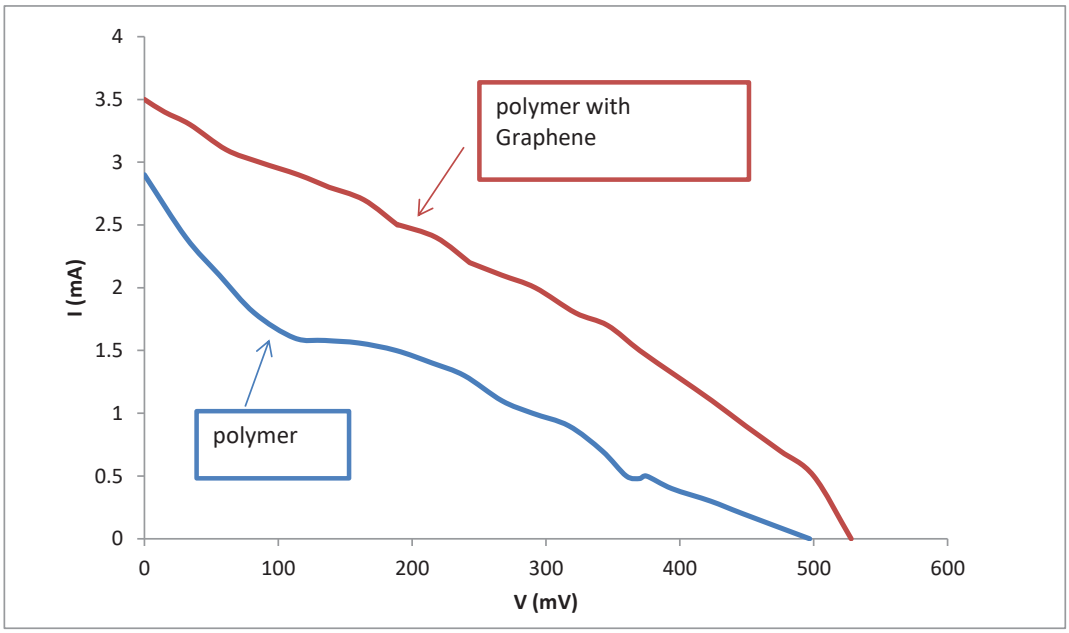


Fig. 9. I-V characteristic for DSSC.

counter electrodes and different active anodes have been subjected to the I-V characterization by fast scan with two electrodes, potentiostate, to calculate all parameters of every one of them; current short circuit (Isc), voltage of open circuit ($V_{oc}$), max cell power ($P_{max}=I_m*V_m$), have been estimated with the use of two electrodes potentiostatic measurements, then the full factor (FF),and conversion efficiency(E%) are calculated by the following equations[24]:

$$E\% = \frac{\text{Voc Isc FF}}{\text{Pinc.}} \quad (1)$$

$$FF = \frac{\text{ImVm}}{\text{Isc Voc}} \quad (2)$$

I-V characteristic is measured by two types of electrodes, poly Tyramide derivative and poly Tyramide derivative modified with Graphene as shown in Fig. 9. Adding of Graphene to poly Tyramide derivative matrix improves the catalytic properties of poly Tyramide derivative. Table shows that DSSCs based on poly Tyramide derivative modified with graphene show higher efficiency than non-modified polymer. Since the high resistance of the poly Tyramide modified with Graphene would obstruct the electrons transport from external circuit to electrolyte, less reduction of $I_3$ to I- is obtained [24]. All values of assemble DSSCs are listed in Table 3.

## CONCLUSION

In summary, the synthesized poly(tyramide derivative) film was successfully polymerized, as confirmed by the disappearance of the aliphatic C=CH stretch at 1616 $cm^{-1}$ in FTIR spectra, alongside SEM revealing a compact morphology that evolves into clustered and fibrous structures upon graphene incorporation. AFM analysis demonstrated increased surface roughness due

to graphene agglomeration, while XRD patterns exhibited crystalline peaks at 2θ = 9.58°, 26.6°, and 28.56° for the polymer, shifting to a broad interaction peak at ~26° with graphene, indicative of strong matrix-sheet interfacial bonding that boosts conductivity. The graphene-modified poly(tyramide derivative) counter electrode in DSSCs yielded higher short-circuit current (Isc), open-circuit voltage (Voc), fill factor (FF), and power conversion efficiency (η) compared to the unmodified polymer, attributed to improved catalytic reduction of $I_3^-$ to $I^-$ despite minor charge transport resistance, positioning this composite as a promising, cost-effective alternative for efficient dye-sensitized solar cells.

## CONFLICT OF INTEREST

The authors declare that there is no conflict of interests regarding the publication of this manuscript.

## REFERENCES


1. Koczkur K, Yi Q, Chen A. Nanoporous Pt-Ru Networks and Their Electrocatalytical Properties. Adv Mater. 2007;19(18):2648-2652.
2. Briscoe J, Dunn S. The Future of Using Earth-Abundant Elements in Counter Electrodes for Dye-Sensitized Solar Cells. Adv Mater. 2016;28(20):3802-3813.
3. Saranya K, Rameez M, Subramania A. Developments in conducting polymer based counter electrodes for dye-sensitized solar cells – An overview. Eur Polym J. 2015;66:207-227.
4. Cho W, Lim J, Kim T-Y, Kim YR, Song D, Park T, et al. Electron-Transfer Kinetics through Interfaces between Electron-Transport and Ion-Transport Layers in Solid-State Dye-Sensitized Solar Cells Utilizing Solid Polymer Electrolyte. The Journal of Physical Chemistry C. 2016;120(5):2494-2500.
5. Marinado T, Hagberg DP, Hedlund M, Edvinsson T, Johansson EMJ, Boschloo G, et al. Rhodaninedyes for dye-sensitized solar cells : spectroscopy, energy levels and photovoltaic performance. Phys Chem Chem Phys. 2009;11(1):133-141.
6. Liu G, Klein A, Thissen A, Jaegermann W. Electronic properties and interface characterization of phthalocyanine and Ru-polypyridine dyes on $TiO_2$ surface. Surface Science. 2003;539(1-3):37-48.
7. Senthilarasu S, Velumani S, Sathyamoorthy R, Subbarayan A, Ascencio JA, Canizal G, et al. Characterization of zinc phthalocyanine (ZnPc) for photovoltaic applications. Appl Phys A. 2003;77(3-4):383-389.
8. Velten J, Mozer AJ, Li D, Officer D, Wallace G, Baughman R, et al. Carbon nanotube/graphene nanocomposite as efficient counter electrodes in dye-sensitized solar cells. Nanotechnology. 2012;23(8):085201.
9. Abdelhameed RM, El Radaf IM. Self-cleaning lanthanum doped cadmium sulfide thin films and linear/nonlinear optical properties. Materials Research Express. 2018;5(6):066402.
10. Ali Alsammarraie AM. Morphology Effect of Anodized $TiO_2$ Nanotubes Active Anodes on Dye Sensitive Solar Cell. Asian J Chem. 2017;29(9):1985-1989.
11. M. Abed G. Cr-Gd co-doped $TiO_2$ Nanoribbons as Photoanode in Making Dye Sensitized Solar Cell. Nanoscience and Nanometrology. 2017;3(1):27.
12. Sana AH, Khulood AS. Electrochemical Polymerization and Biological Activity of 4-(Nicotinamido)-4-Oxo-2-Butenoic Acid as An Anticorrosion Coating on A 316L Stainless Steel Surface. Iraqi Journal of Science. 2021:729-741.
13. Aradilla Zapata D. Design, synthesis, characterization and development of novel organic conducting polymers with technological applications: Universitat Politècnica de Catalunya.
14. Giessibl FJ. Advances in atomic force microscopy. Rev Mod Phys. 2003;75(3):949-983.
15. Dirghangi A, Mohanty S. De-mythifying the Ramayana: A Study of the 'Devoiced' Surpanakha. International Conference on Arts and Humanities; 2020/01/20: The International Institute of Knowledge Management; 2020. p. 08-15.
16. Stephen WI. H.H. Willard, L.L. Merritt Jr. and J.A. Dean, Instrumental methods of analysis. Anal Chim Acta. 1967;39:407.
17. Hoard JL. X-Ray Crystallography:X-Ray Crystallography. An Introduction to the Investigation of Crystals by their Diffraction of Monochromatic X-Radiation. By M. J. Buerger, associate professor of mineralogy and crystallography, Massachusetts Institute of Technology. xxii + 531 pp. New York: John Wiley and Sons, 1942. $6.50. Science. 1944;99(2568):223-223.
18. Peiser HS. X-Ray Diffraction in Crystals, Imperfect Crystals, and Amorphous Bodies. A. Guinier. Translated from the French edition (Paris, 1956) by Paul Lorrain and Dorothee Sainte-Marie Lorrain. Freeman, San Francisco, 1963. x + 378 pp. Illus. $11. Science. 1963;142(3599):1564-1564.
19. Nethravathi C, Rajamathi M, Ravishankar N, Basit L, Felser C. Synthesis of graphene oxide-intercalated α-hydroxides by metathesis and their decomposition to graphene/metal oxide composites. Carbon. 2010;48(15):4343-4350.
20. Dhole SG, Dake SA, Prajapati TA, Helambe SN. Effect of ZnO Filler on Structural and Optical Properties of Polyaniline-ZnO Nanocomposites. Procedia Manufacturing. 2018;20:127-134.
21. Vaishnav D, Goyal RK. Thermal and Dielectric Properties of High Performance Polymer/ZnO Nanocomposites. IOP Conference Series: Materials Science and Engineering. 2014;64:012016.
22. Valença DP, Alves KGB, Melo CPd, Bouchonneau N. Study of the Efficiency of Polypyrrole/ZnO Nanocomposites as Additives in Anticorrosion Coatings. Materials Research. 2015;18(suppl 2):273-278.
23. Alzari V, Nuvoli D, Sanna R, Scognamillo S, Piccinini M, Kenny JM, et al. In situ production of high filler content graphene-based polymer nanocomposites by reactive processing. J Mater Chem. 2011;21(41):16544.
24. Sarwar S, Park S, Dao TT, Lee M-s, Ullah A, Hong S, et al. Scalable photoelectrochromic glass of high performance powered by ligand attached $TiO_2$ photoactive layer. Sol Energy Mater Sol Cells. 2020;210:110498.